Expanded View Figures

Figure EV1. The C terminus of ATG9A harbors hallmarks of a signaling hub and is involved in self-association, and ATG9A trafficking.

A Graph showing disorder tendency of ATG9A across its amino acid sequence (predicted by ANCHOR web server at http://anchor.elte.hu/) and PTM distribution across the protein quantified by High Throughput Paper (HTP) observations (generated by PhosphoSitePlus® at https://www.phosphosite.org/psrSearchAction) (top). Schematic of ATG9A domain structure (bottom).

B Schematic representation showing N- or C-terminal halves of mVenus fused to C terminus of ATG9A (top left). HCT-116 cells expressing ATG9A C-terminally labeled N mVenus or N + C mVenus constructs were grown in full DMEM media, fixed, and imaged (Scale bar = 10 μm) (right). Fluorescence intensity of cells expressing ATG9A C-terminally labeled mVenus constructs was measured via flow cytometry. Mean ± SEM, $n = 1$(bottom left).

C Hela ATG9A WT, ATG9A KO, or ATG9A KO cells reconstituted with ATG9A WT and ATG9A ΔC mutant stably expressing GFP-LC3 were grown in full media and whole-cell lysates followed by immunoblotting with indicated antibodies (left). Quantification of normalized GFP and normalized LCII/LC3I ratio. Mean ± SEM, $n = 3$ (biological replicates). Significance measured using RM one-way ANOVA followed by Fisher's LSD tests. $^{ns}P > 0.05$, $^{*}P \leq 0.05$, $^{**}P \leq 0.01$, $^{***}P \leq 0.001$, $^{****}P \leq 0.0001$.

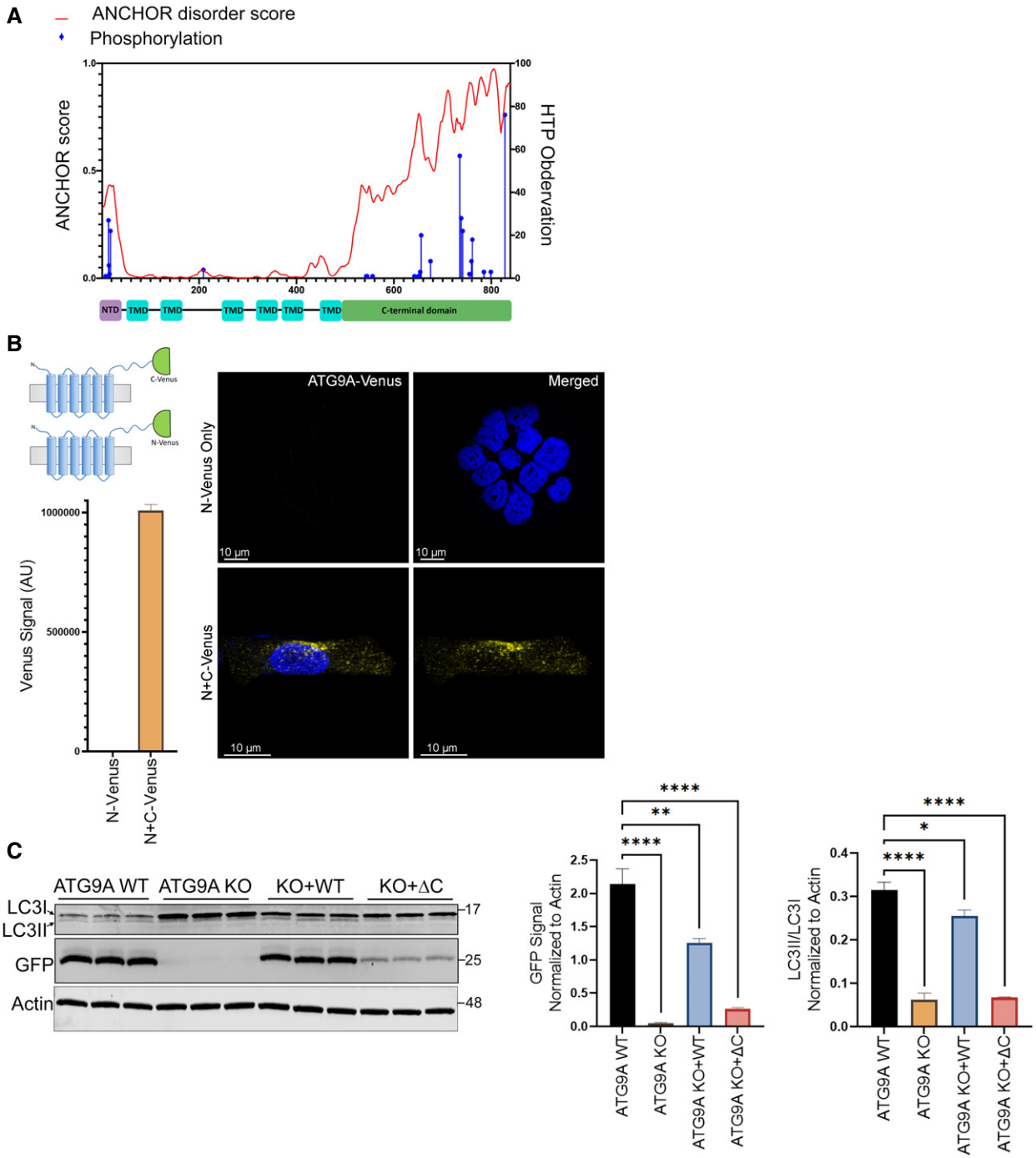

Figure EV1.

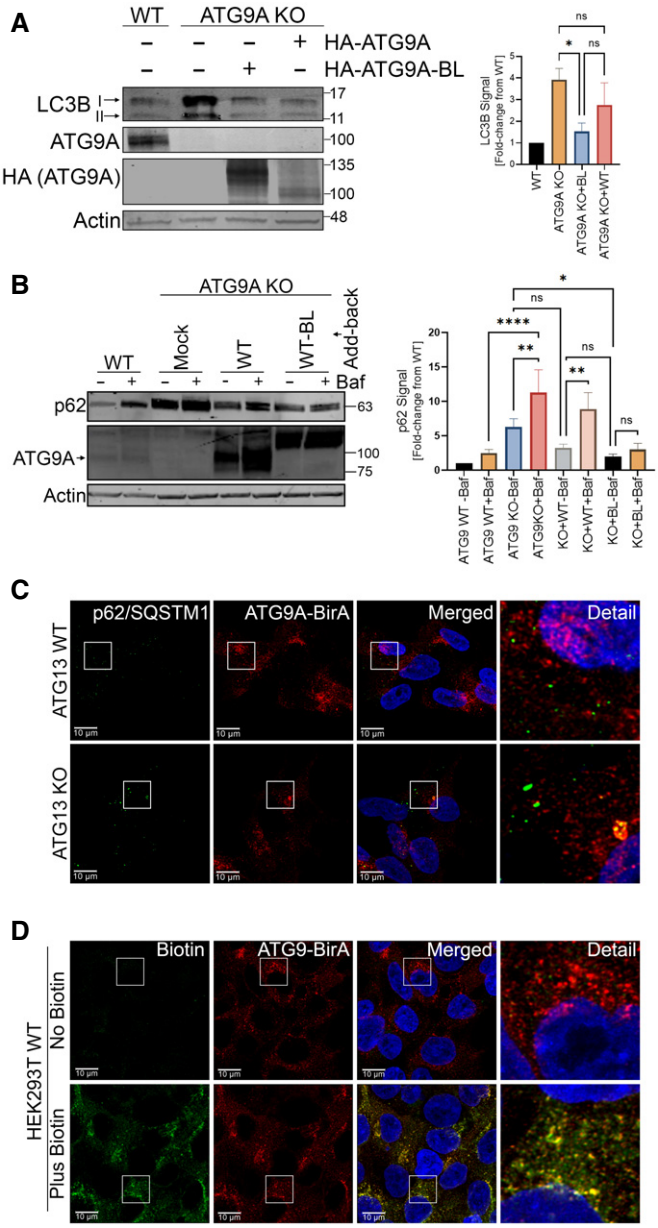

Figure EV2. Functional validation of HA-ATG9A-BirA* constructs.

A HEK293T WT, ATG9A KO, and ATG9A KO cells reconstituted with HA-ATG9A and HA-ATG9A-BirA* were grown in full DMEM media, lysed, and immunoblotted with indicated proteins (left). Quantification of normalized LC3B infrared signal. Mean ± SEM, $n = 3$ (biological replicates). Significance measured using RM one-way ANOVA followed by Fisher's LSD tests (right).

B HEK293T WT, ATG9A KO, and ATG9A KO cells reconstituted with HA-ATG9A and HA-ATG9A-BirA* were grown in full DMEM media with or without 100nM Bafilomycin for 24 h, lysed, and immunoblotted with indicated proteins (left). Quantification of normalized p62 infrared signal. Mean ± SEM, $n = 3$ (biological replicates). Significance measured using RM one-way ANOVA followed by Fisher's LSD tests (right).

C Confocal images of p62/SQSTM1 colocalization with HA-ATG9A-BirA* in HEK293T ATG13 WT and ATG13 KO cells stably expressing HA-ATG9A-BirA*. Cells were grown in full DMEM media, fixed, and labeled with antibodies for p62/SQSTM1 and HA (Scale bar = 10 µm).

D Confocal images of biotinylated proteins colocalized with HA-ATG9A-BirA*. HA-ATG9A-BirA*-expressing cells were grown in full DMEM media with or without biotin incubation (12 h), fixed, and labeled with Alexa Fluor 488-conjugated streptavidin and HA antibody (Scale bar=10 µm). $^{ns}P > 0.05$, $^{*}P \leq 0.05$, $^{**}P \leq 0.01$, $^{***}P \leq 0.001$, $^{****}P \leq 0.0001$.

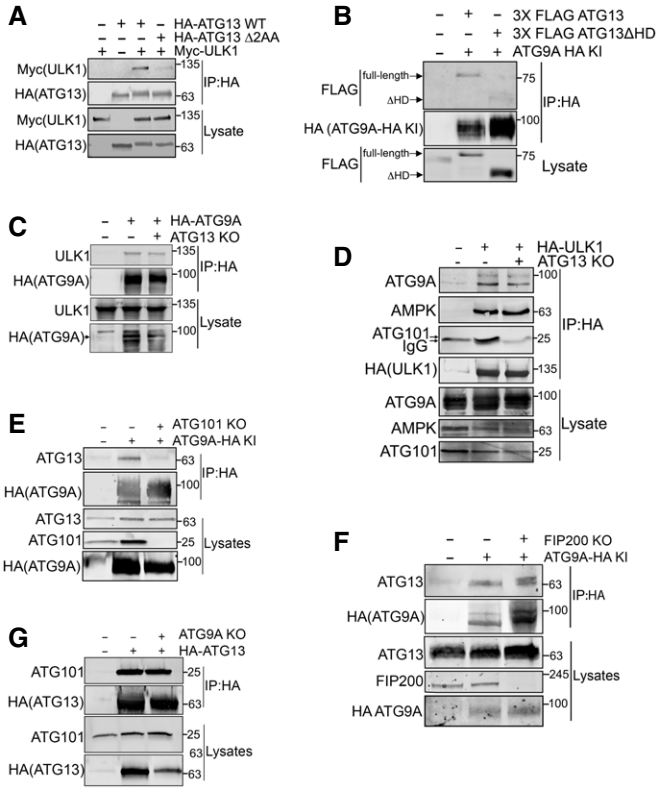

Figure EV3. ATG9A interacts with an ULK1-independent ATG13-ATG101 subcomplex via the ATG13 HORMA domain.

A The ULK1 binding-deficient mutant of ATG13 (ATG13 Δ2AA) was validated by immunoprecipitating HA-ATG13 or HA-ATG13 Δ2AA and immunoblotting for Myc-ULK1 in HCT-116 ATG13 KO cells.

B HCT-116 parental or HCT-116 ATG9A-HA KI ATG13 KO cells reconstituted with 3X FLAG-ATG13 WT or 3X FLAG-ATG13 ΔHORMA were grown in full DMEM media and subjected to size exclusion chromatography. Fractions with high levels of ATG9A-HA were pooled to facilitate immunoprecipitation. ATG9A-HA was immunoprecipitated from pooled fractions followed by immunoblotting with indicated antibodies.

C Co-IP of overexpressed HA-ATG9A from HCT-116 ATG13 KO cells followed by immunoblotting with indicated antibodies.

D Co-IP of HA-ULK1 from HCT-116 ATG13 WT and KO cells followed by immunoblotting with indicated antibodies.

E Co-IP of endogenous ATG9A from HCT-116 ATG9A-HA KI ATG101 KO cells followed by immunoblotting with indicated antibodies.

F Co-IP of endogenous ATG9A from HCT-116 ATG9A-HA KI FIP200 KO cells followed by immunoblotting with indicated antibodies.

G Co-IP of overexpressed HA-ATG13 from HEK293T ATG9A KO cells followed by immunoblotting with indicated antibodies.

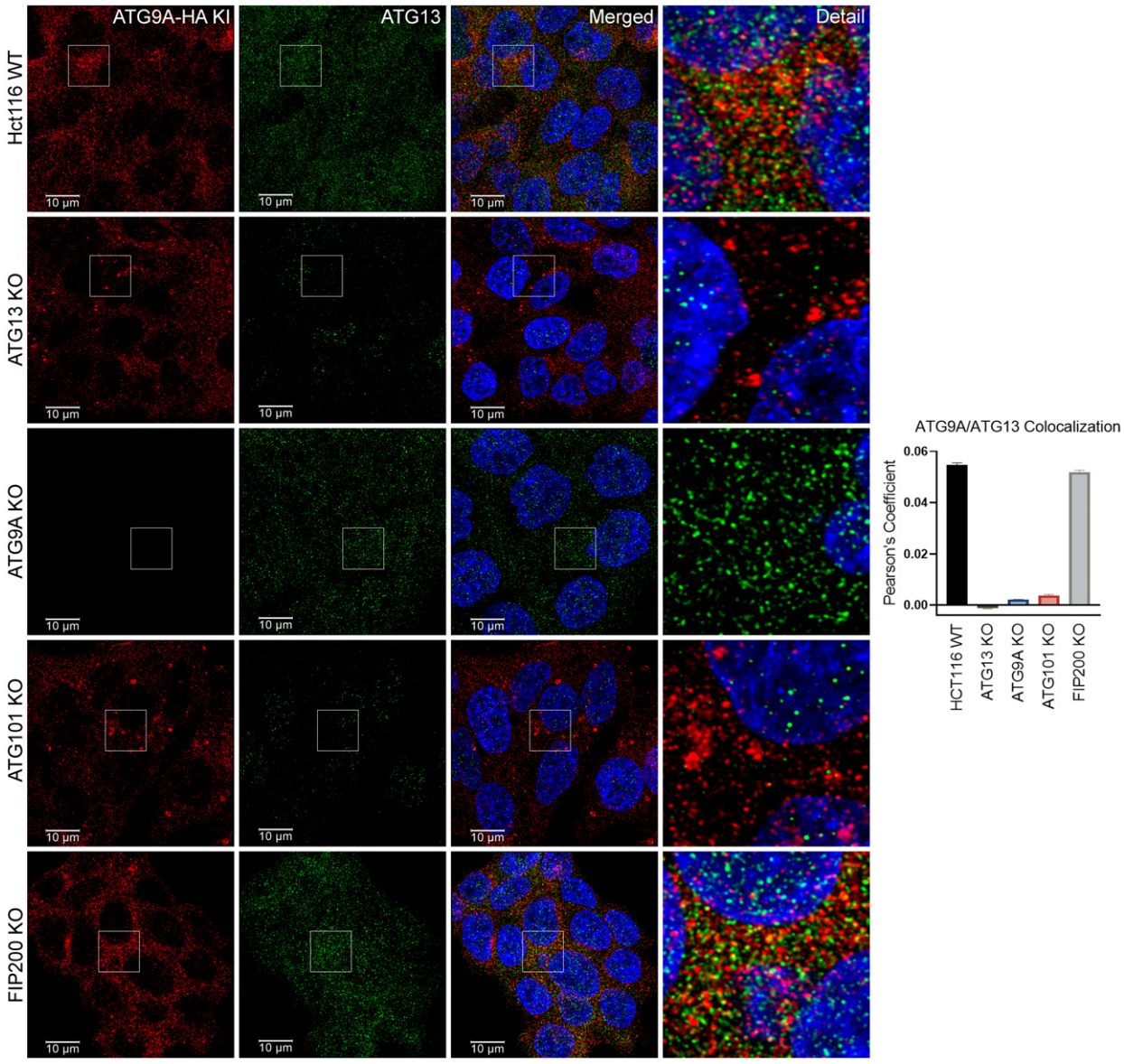

Figure EV4. ATG13 colocalization with ATG9A is independent of FIP200/ULK1 complex.

HCT-116 ATG9A-HA KI ATG13 WT, ATG13 KO, ATG101 KO, ATG9A KO, and FIP200 KO cells were grown in full DMEM media, fixed, labeled with antibodies for HA and ATG13, and imaged (Scale bar = 10 µm) (left). Quantification of ATG9A colocalization with ATG13. Mean ± SEM, $n = 1$ independent experiment with 30 technical replicates. Images are derived from the same experiment as Fig EV5 and Appendix Fig S3.

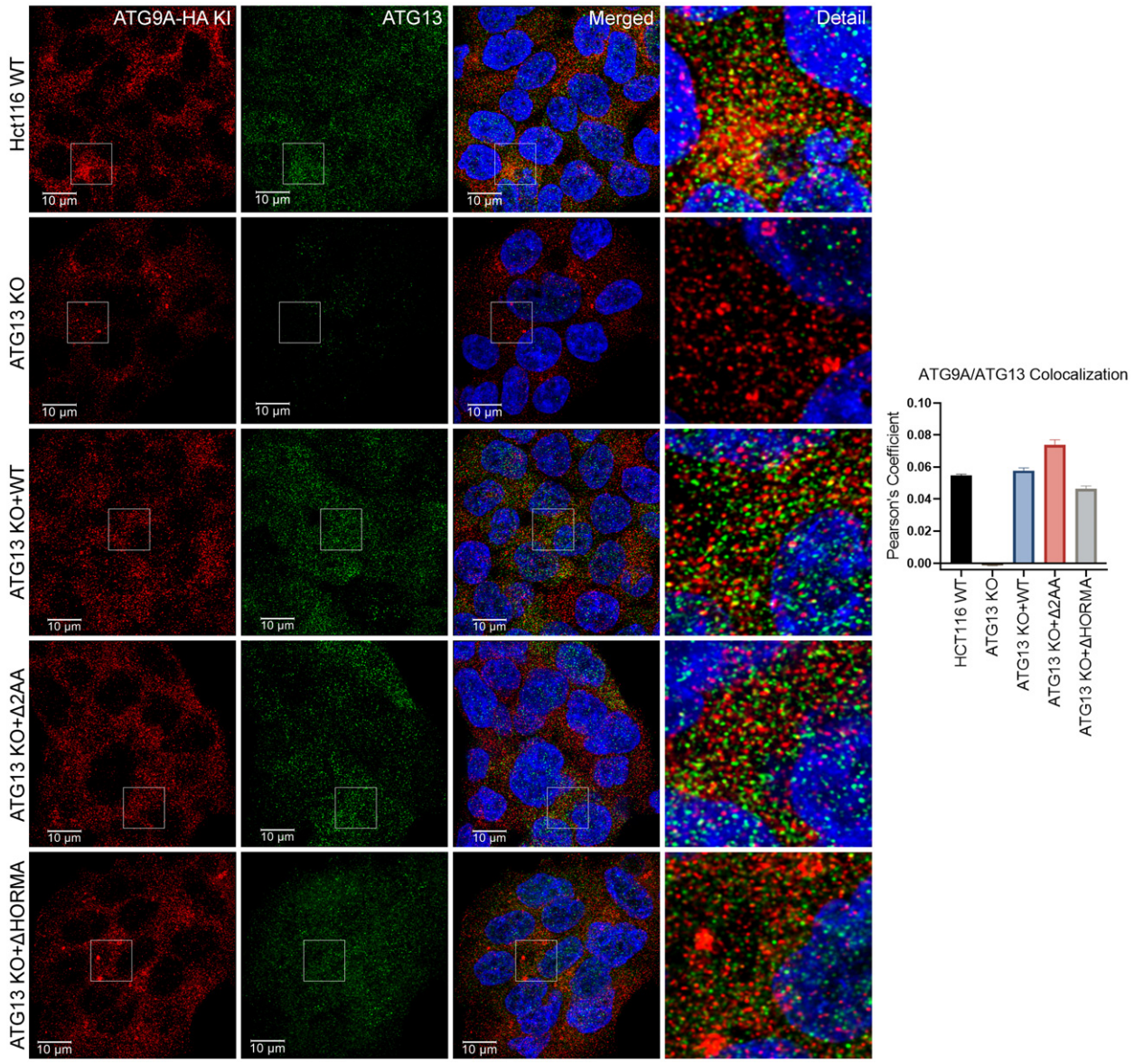

Figure EV5. ATG13 colocalization with ATG9A requires the ATG13 HORMA domain, but occurs independently of ULK1 binding.

A, B HCT-116 ATG9A-HA KI ATG13 WT, ATG13 KO or ATG13 KO cells reconstituted with ATG13 WT, ATG13 Δ2AA, and ATG13 ΔHORMA. Cells were grown in full DMEM media, fixed, labeled with antibodies for HA and ATG13, and imaged. (Scale bar = 10 μm).

C Quantification of ATG9A colocalization with ATG13. Mean ± SEM, n = 1 independent experiment with 30 technical replicates. Images are derived from the same experiment as Fig EV4 and Appendix Fig S3.

